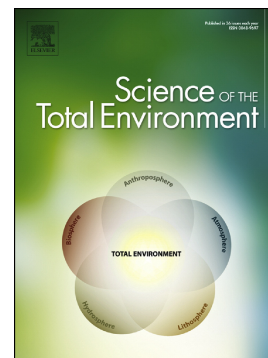


## Accepted Manuscript

Application of hardwood biochar as a reactive capping mat to stabilize mercury derived from contaminated floodplain soil and riverbank sediments

Alana O. Wang, Carol J. Ptacek, David W. Blowes, Blair D. Gibson, Richard C. Landis, James A. Dyer, Jing Ma



PII: S0048-9697(18)34104-4  
DOI: [doi:10.1016/j.scitotenv.2018.10.213](https://doi.org/10.1016/j.scitotenv.2018.10.213)  
Reference: STOTEN 29116

To appear in: *Science of the Total Environment*

Received date: 10 August 2018  
Revised date: 14 October 2018  
Accepted date: 15 October 2018

Please cite this article as: Alana O. Wang, Carol J. Ptacek, David W. Blowes, Blair D. Gibson, Richard C. Landis, James A. Dyer, Jing Ma , Application of hardwood biochar as a reactive capping mat to stabilize mercury derived from contaminated floodplain soil and riverbank sediments. Stoten (2018), doi:[10.1016/j.scitotenv.2018.10.213](https://doi.org/10.1016/j.scitotenv.2018.10.213)

This is a PDF file of an unedited manuscript that has been accepted for publication. As a service to our customers we are providing this early version of the manuscript. The manuscript will undergo copyediting, typesetting, and review of the resulting proof before it is published in its final form. Please note that during the production process errors may be discovered which could affect the content, and all legal disclaimers that apply to the journal pertain.

Application of Hardwood Biochar as a Reactive Capping Mat to Stabilize Mercury  
Derived from Contaminated Floodplain Soil and Riverbank Sediments

Alana O. Wang<sup>a</sup>, Carol J. Ptacek<sup>\*a</sup>, David W. Blowes<sup>a</sup>, Blair D. Gibson<sup>b</sup>, Richard C.  
Landis<sup>c1</sup>, James A. Dyer<sup>c2</sup>, Jing Ma<sup>b3</sup>

<sup>a</sup> Department of Earth and Environmental Sciences, University of Waterloo, Waterloo,  
ON, Canada, N2L 3G1

<sup>b</sup> formerly at Department of Earth and Environmental Sciences, University of Waterloo,  
Waterloo, ON, Canada, N2L 3G1

<sup>c</sup> formerly at E.I. du Pont de Nemours and Company, Wilmington, DE, USA, 19085

---

\*Corresponding author: Carol J. Ptacek  
Email: [ptacek@uwaterloo.ca](mailto:ptacek@uwaterloo.ca)  
Tel: 1-519-888-4567 ex. 32230

<sup>1</sup> Currently at RichLand Consulting, LLC, Lincoln University, PA, USA

<sup>2</sup> Currently at Savannah River National Laboratory, Aiken, SC, USA, 29808

<sup>3</sup> Currently at SGS Canada, Mississauga, ON, Canada

## Abstract

Hardwood biochar (pyrolyzed at 700 °C), a potential candidate for Hg removal, has been proposed for use as reactive capping mat along groundwater discharge zones or riverbanks to control release of Hg from contaminated riverbank sediments. Frequent flooding and drainage in fluvial settings can influence the effectiveness of remediation systems in contaminated riverbank sediments and floodplain soils. This study evaluated the effectiveness of Hg removal using hardwood biochar under hydrogeochemical conditions representative of those present within a reactive capping mat installed in a fluvial setting. Two sets of treatment columns, containing 50% v.v biochar and quartz sand, were subjected to 100 weekly wetting/drying cycles that included dry air, water-saturated air, and drainage using leachate derived from two source columns as input solutions: 1. Passing simulated acid rain water through floodplain soil, 2. Passing river water through riverbank sediment. In both treatment columns, more than 80% of the Hg was retained on the biochar without promoting Hg methylation and the release of other unintended dissolved constituents (including N, P, DOC). Results from solid phase extraction analyses suggest that Hg accumulated near the air/biochar-sand interface (0-2 cm) in the treatment columns at low loadings but was present at greater depths at higher loadings. Results of micro X-ray fluorescence ( $\mu$ -XRF) mapping and micro X-ray absorption near edge structure ( $\mu$ -XANES) for the biochar collected at depths 0-2 cm in treatment columns suggest retention of Hg-bearing particles derived from riverbank sediment and floodplain soil within the pore structure of the biochar. Sulfur K-edge XANES analyses of the unused biochar and biochar after treatment suggest formation

of Hg complexes on the biochar surface. Based on these results, hardwood biochar is potentially an effective media for application in reactive mats for controlling Hg discharging from contaminated riverbank sediments.

**Keywords:**

Mercury stabilization; Fluvial soil remediation; X-ray absorption near edge structure (XANES); Micro X-ray fluorescence ( $\mu$ -XRF) maps

## 1 Introduction

Mercury contamination in river water related to industrial activities has been widely documented around the world (Carter, 1977; Kocman et al., 2013; Morway et al., 2017). The release of Hg compounds to riverine systems can result in extensive accumulations of Hg in surrounding riverbank sediment and floodplain soils (Carter, 1977; Eggleston, 2009; Flanders et al., 2010; Mucci et al., 2015, Morway et al., 2017). Under reducing conditions, microorganisms in streams and soil pore water can methylate inorganic Hg species, such as nanoparticulate HgS, dissolved Hg(II), and dissolved Hg<sup>(0)</sup>, to methylmercury (MeHg) in the presence of organic matter, posing health risks to humans and wildlife (Desrochers et al., 2015; Gilmour et al., 2013a; Guedron et al., 2011; Hu et al., 2013; Liu et al., 2016, 2018; Mosher et al., 2012; Paulson et al., 2016).

Mercury accumulates in alluvial sediments and floodplain soils mainly by adsorption on soil organic matter and Fe oxides (Mucci et al., 2015; Pizzuto, 2012). The release of Hg to pore water is controlled by multiple processes, including the release of suspended particles, release of particulate HgS, degradation of soil organic matter, reductive dissolution of Hg-rich Fe-oxides, and reduction of nanoparticulate metacinnabar ( $\beta$ -HgS) to Hg<sup>(0)</sup><sub>aq</sub> (Babiarz et al., 2012; Gibson et al., 2015; Hofacker et al., 2013; Lowry et al., 2004; Mucci et al., 2015; Poulin et al., 2016).

Frequent hydrological changes in fluvial settings can result in shifts in biogeochemical conditions, thus affecting the dynamic Hg cycle. During high runoff events, upstream soil erosion leads to increases in the release of suspended particles, thus causing the remobilization of Hg to river water associated with clay particles

(Babiarz et al., 2012). Natural resuspension of sediments in freshwater bodies under oxic conditions can also result in the release of Hg to river water (Gibson et al., 2015). During extended inundation conditions, dissolved O<sub>2</sub> originally trapped within sediment pore spaces can be rapidly consumed by organic matter oxidation. Under these reducing conditions, mercury release to pore-water is controlled by rates of soil organic matter degradation and reductive dissolution of reactive Fe-oxides, among other processes (Mucci et al., 2015; Poulin et al., 2016). Periods of extended flooding provide favourable conditions for methylation reactions at the sediment-water interface, mainly related to increases in bacterial activity (Johnson et al., 2010; Poulin et al., 2016; Singer et al., 2016).

Recent studies on in situ Hg stabilization focus on soil amendments for immobilizing Hg and minimizing production of MeHg (Bundschuh et al., 2015; Gilmour et al., 2013b, 2018; Gomez-Eyles et al., 2013; Li et al., 2018; Liu et al., 2017, 2018; Wang et al., 2019; Zhang et al., 2018). Biochar, produced from natural raw organic materials with relatively large surface areas and abundant surface functionalities, has been widely evaluated as an alternative Hg immobilizing reagent due to its relatively low-cost and potential for local availability (Bundschuh et al., 2015; Gilmour et al., 2018; Gomez-Eyles et al., 2013; Liu et al., 2017, 2018; Zhang et al., 2018). Studies on Hg stabilization using biochar indicate biochar can reduce net MeHg production (Bundschuh et al., 2015; Gilmour et al., 2018; Gomez-Eyles et al., 2013; Liu et al., 2017, 2018; Zhang et al., 2013) as well as control the release of Hg from sediments (Liu et al., 2017, 2018).

Management of Hg release from riverbank sediments and floodplain soils is challenging due to the complexity of processes controlling the release and

transformation of Hg. Mercury contamination at the watershed scale is usually distributed at isolated locations in a relatively large catchment (Flanders et al., 2010). Direct application of biochar as a soil amendment at isolated locations in a watershed scale may not be effective due to erosional losses caused by frequent flooding and drainage in riverine environments (Gilmour et al., 2018). Installing engineered reactive passive mats containing biochar as reactive materials along riverbanks has been proposed as a solution to retain biochar in designated locations and stabilize Hg under saturated flow conditions (Desrochers, 2013; Paulson 2014). The long-term effectiveness of Hg removal using reactive mats under flooding and drainage conditions is unclear. An evaluation of the robustness of the reactive mat is essential before installing in the field at larger scales.

Based on a previous 48-hour batch study, the hardwood biochar (pyrolyzed at 700°C) was selected due to its relatively high surface area and abundant surface functionalities, and low concentrations of  $\text{SO}_4^{2-}$  and organic acids compared to agricultural residue and manure-based biochars (Liu et al., 2015). The batch-scale experiments evaluating the hardwood biochar also show Hg removal that is similar to the removal observed using commercial activated carbon, but slightly less than agriculture residue biochars and manure-based biochars (Liu et al., 2016). However, due to the relatively low concentrations of  $\text{SO}_4^{2-}$ , DOC and acetate, the selected hardwood biochar, is less likely to promote Hg methylation in contaminated sediments under fully saturated static conditions (Liu et al., 2018), and in experiments designed to evaluate a reactive capping mat under saturated flow conditions (Desrochers, 2013; Paulson, 2014). The effectiveness of biochar to stabilize Hg in fluvial settings, where

frequent changes in hydrogeological and biogeochemical conditions occur, has not been widely evaluated.

This study evaluated the long-term effectiveness of Hg removal derived from riverbank sediment and floodplain soil using hardwood biochar as a passive reactive capping mat. Floodplain soils and sediments were used in laboratory apparatus modified from a standard humidity cell test method to provide the input source water for the experiment. Effluent from the source columns was directed to humidity test cells containing treatment materials. This configuration mimicked field weathering conditions and placement of reactive media representative of typical riverine systems.

## 2 Study Site

The South River, located in the Shenandoah Valley in Virginia, starts to the south of Stanton, passes through Waynesboro, and flows to north of Port Republic before it joins the South Fork Shenandoah River (Figure A 1). A textile plant in Waynesboro, VA, used  $\text{HgSO}_4$  as a catalyst to manufacture acetate fiber from 1929 to 1950. In the 1970s, elevated concentrations of Hg were observed in South River water, downstream soil samples, and fish tissue (Carter, 1977). Bank erosion has been postulated to be the primary source of Hg release from the alluvial sediments in the South River watershed to freshwater bodies downstream, corresponding to an estimated minimum annual input rate of  $109.6 \text{ kg year}^{-1}$  (Eggleston, 2009; Rhoades et al., 2009). Concentrations of inorganic particulate Hg of up to  $29.9 \mu\text{g g}^{-1}$  have been observed 16 km downstream from the historical release site (Flanders et al., 2010). Sulfate- and iron-reducing

bacteria present in the riverbank sediments and floodplain soils contribute to the net production of MeHg (Desrochers et al., 2015; Paulson et al., 2016; Yu et al., 2012).

### **3 Material and Methods**

#### **3.1 Materials**

Hardwood biochar, prepared from oak and maple hardwood and pyrolyzed at approximately 700 °C, was obtained from Cowboy Charcoal LLC (Brentwood, TN, USA). The biochar was sieved between 0.5 and 2 mm. Riverbank sediment (SR6) was collected from the unsaturated zone of the South River from a depth of 0.3 m below ground surface at a location 0.16 km downstream from the point of historical Hg release; floodplain soil (MOTO) was collected from the center of a cut-off floodplain located 1.65 km downstream from the historical release site (Figure A 1, Table A 1). The riverbank sediments and floodplain soils were shipped to the University of Waterloo and stored below 4 °C before use. The South River water (SRW) used in the experiment was collected upstream of the historical Hg release site on a bimonthly basis and shipped on ice to the University of Waterloo. SRW was stored at 4 °C and in dark conditions prior to utilization in the experiment. Simulated acid rain water (ARW) was prepared by diluting a stock solution of 1 M H<sub>2</sub>SO<sub>4</sub> and 1.14 M HNO<sub>3</sub> to a final pH of 4.6.

#### **3.2 Experimental design**

The humidity-cell-test method is a standardized laboratory procedure to evaluate the release of metals from mine wastes using a fixed-volume of aqueous leaching solution under simulated weathering conditions (Ardau et al., 2009; ASTM, 2012; Langman et al., 2015a, 2015b; Maest and Nordstrom., 2017; Wilson et a., 2018). The first week of the

test method includes adding three aliquots of ultrapure water to remove by-products generated during storage. Subsequent weekly cycles start with dry air, water-saturated air at 22 °C, and the addition of an aliquot of ultrapure water at the end of each week that is drained by gravity.

In this study, minor modifications were made to the standard method. Acrylic columns were downscaled and had dimensions of 7.4 × 15.3 cm. Two source columns were packed with contaminated sediments that were leached under cyclic wetting/drying conditions. The leachate from the source columns was collected and used as the input solution for subsequent treatment columns that also were subjected to cyclic wetting/drying conditions (Figure 1). One source column (HMT) was packed with MOTO. Sediments at the MOTO site are subject to acid precipitation, therefore ARW was used as the input solution for HMT. Weekly cycles started with 3 d dry air, 4 d water-saturated air, and the addition of 125 mL ARW on day 7 of each week. The other source column (H6S) was packed with SR6 and had SRW as the input solution; its weekly cycle started with 1 d dry-air, 1 d water-saturated air, then 125 mL SRW added to the column on day 3 of each week. SRW was held in the column for 4 d to represent flooding conditions. On day 7, the leachate was drained by gravity and an aliquot collected for analysis, with the remaining volume used as the input solution for the treatment columns. The treatment columns were packed with 50% v/v biochar and quartz sand and flushed with three 125-mL aliquots of ultrapure water during the first week to remove fine ash on the biochar. Aliquots of leachate collected from HMT and H6S were used as the input solutions for treatment humidity cells THC-HMT and THC-H6S, respectively. The weekly cycle for the treatment columns started with dry air (3 d

for THC-HMT and 1 d for THC-H6S), water-saturated air (4 d for THC-HMT and 5 d for THC-H6S), then 100 mL of leachate from HMT or H6S on day 7. Treatment effluents were drained by gravity on day 7 and collected for analysis.

### 3.3 Effluent sample collection

Effluent samples were collected in 250-mL Erlenmeyer flasks washed in 20% HCl. Samples for pH, Eh, total alkalinity, total Hg (THg), methylmercury (MeHg), cations, anions, dissolved organic carbon (DOC), NH<sub>3</sub>-N, and PO<sub>4</sub>-P were collected using 20-mL polypropylene/ polyethylene sterile Luer lock syringes (Norm-Ject, Thermo Fisher Scientific, Burlington, ON, Canada). pH and Eh were determined on unfiltered samples shortly after collection. Samples for analysis of total alkalinity, THg, MeHg, cations, anions, DOC, NH<sub>3</sub>-N, and PO<sub>4</sub>-P were passed through 32-mm diameter syringe filters with 0.45- $\mu$ m Supor<sup>®</sup> membranes (Acrodisc<sup>®</sup>, VWR, Burlington, ON, Canada). Unfiltered samples were also collected for THg and MeHg analyses in 15-mL vacuum and ionized amber borosilicate-glass vials with PTFE-lined caps (Qorpak<sup>®</sup>, VWR, Mississauga, ON, Canada). Samples for cation and anion analysis were collected in 15-mL polypropylene copolymer bottles (Nalgene<sup>®</sup>, VWR, Mississauga, ON, Canada). Samples for DOC, NH<sub>3</sub>-N, and PO<sub>4</sub>-P were collected in 15-mL amber borosilicate-glass vials with PTFE-lined caps. All samples, except for anion samples, were acidified to pH < 2 as follows: samples for THg and cations with ACS reagent grade 15.6 N HNO<sub>3</sub> (JT Baker<sup>®</sup>, VWR, Mississauga, ON, Canada); samples for MeHg with ACS reagent grade 12.1 N HCl (JT Baker<sup>®</sup>, VWR, Mississauga, ON, Canada); and samples for DOC, NH<sub>3</sub>-N, and PO<sub>4</sub>-P with OmniTrace Ultra<sup>™</sup> 18.4 M H<sub>2</sub>SO<sub>4</sub> (MilliporeSigma, VWR, Mississauga, ON, Canada). All samples were stored at < 4 °C before analyses.

### 3.4 Solid sample collection

After 100 subsequent cycles, the treatment humidity cells (THC-HMT and THC-H6S) were sectioned into 2-cm intervals downward from the air/biochar-sand interface to the bottom of the column in a 3.5% H<sub>2</sub>/balanced N<sub>2</sub> vinyl anaerobic chamber (COY, Mandel Scientific Company, Guelph, ON, Canada) to avoid further oxidation. The solid samples were frozen at -20 °C prior until further analyses. Solid-phase samples collected at depths of 0-2, 2-4, 4-6, and 6-8 cm from the treatment columns were used for a five-step sequential extraction procedure, THg digestion, MeHg extraction, and S K-edge X-ray absorption near edge structure (XANES) analyses. Portions of materials from 0-2 cm were used to prepare polished thin sections for micro X-ray absorption spectroscopy ( $\mu$ -XAS) analysis. The polished thin sections were prepared by mounting freeze-dried biochar particles on 26 × 26 mm quartz slides with thicknesses of 30  $\mu$ m (Vancouver Petrographics Ltd, Vancouver, Canada).

### 3.5 Analytical methods

pH was determined using a combination Ross electrode (Orion model 8156, Thermo Scientific, Waltham, MA, USA) calibrated with standard pH buffers (Thermo Fisher Scientific, Burlington, ON, Canada) at 7.00, 4.00, 10.01 and checked against buffer 7.01 where slopes for three-point calibrations were between 98 and 100%. Eh was determined using a combination platinum Ag/AgCl electrode (Orion 9678, Thermo Scientific, Burlington, ON, Canada) checked against ZoBell's (Nordstrom, 1977) and Light's (Light, 1972) solutions. All Eh values are reported relative to the standard hydrogen electrode. Alkalinity (as CaCO<sub>3</sub> mg L<sup>-1</sup>) was analyzed on 0.45- $\mu$ m filtered samples at the time of sample collection with a digital titrator using standardized 0.16 N

H<sub>2</sub>SO<sub>4</sub> (HACH, VWR, Mississauga, ON, Canada) and with bromocresol-green methyl red as an indicator.

Concentrations of trace elements were determined using inductively coupled plasma mass spectroscopy (ICP-MS, X Series 2, Thermo Scientific), and concentrations of major cations were determined using inductively coupled plasma optical emission spectrometry (ICP-OES, iCAP 6000, Thermo Scientific). Concentrations of anions were determined using ion chromatography (DIONEX™ DX600, Thermo Scientific), with a hydroxide eluent (IonPac AG17 4 mm × 50, AS17 4 mm × 250) used for organic acids (lactate, acetate, propionate, and formate) and a carbonate eluent for major inorganic anions (IonPac AG9-HC 4 mm × 50, AS9-HC 4 mm × 250). DOC was determined using a total organic carbon (TOC) analyzer (TOC-LCPH/CPN, Shimadzu Scientific Instruments, Inc. Columbia, MD, USA) following US EPA method 415.3 (US EPA, 2009). Reactive phosphorus PO<sub>4</sub>-P (orthophosphate) was determined following the ascorbic acid method 4500-P E described in the Standard Methods for Examination of Water and Waste Water (APHA, 2005). Samples for NH<sub>3</sub>-N were neutralized with 5 N NaOH (Hach, VWR, Mississauga, ON, Canada) before analysis. NH<sub>3</sub>-N was determined using LR Test'n Tube™ vials (Hach, VWR, Mississauga, ON, Canada) following the salicylate method (Method 10023 from Hach DR 2800 manual) adapted from Reardon et al. (1966).

THg in different fractions was determined using cold vapor atomic fluorescence spectroscopy (CVAFS, Tekran® 2600, Tekran Instruments Corp, Scarborough, ON, Canada) following US EPA Method 1631 Revision E (US EPA, 2002). Quality assurance/quality control for THg analyses are summarized in supplementary

information (Table A 2). The arithmetic mean for the instrument detection limit was  $0.19 \pm 0.1 \text{ ng L}^{-1}$ . The recovery of certified reference material NIST 1614 D was 97% ( $n > 25$ ). The arithmetic means of the relative percent standard deviation (% R.S.D) for triplicate samples for 0.45- $\mu\text{m}$  and unfiltered THg were 10.7% and 7.82%, respectively. The recovery for matrix spike was 106%.

MeHg was determined using an automated MeHg analyzer (Tekran<sup>®</sup>2700, Tekran Instruments Corp., Scarborough, ON, Canada), after distillation using a temperature-controlled apparatus (Tekran<sup>®</sup>2750, Tekran Instruments Corp, Scarborough, ON, Canada) and ethylating and purging following US EPA Method 1630 (US EPA, 2001). The instrument detection limit was  $0.02 \pm 0.01 \text{ ng L}^{-1}$  ( $n=7$ ), and distillation standard recovery ranged from 83-125%. Matrix spikes ranged from 108-121%.

### 3.6 Calculation of Hg retained on biochar

Hg retained on biochar was estimated using the difference between concentrations of unfiltered Hg in the input solutions and in the treatment effluents, normalized to the masses of biochar in the treatment columns:

$$THg \text{ retained on biochar } (\mu\text{g g}^{-1}) = \frac{(M_{Hg \text{ in}} - M_{Hg \text{ out}})}{M_{\text{biochar}}},$$

$$M_{Hg \text{ in}} (\mu\text{g}) = \sum_{i=1}^{100} C_{\text{input } i} V_{\text{input } i},$$

$$M_{Hg \text{ out}} (\mu\text{g}) = \sum_{i=1}^{100} C_{\text{output } i} V_{\text{output } i},$$

where  $M_{Hg \text{ in}}$  ( $\mu\text{g}$ ) is the mass of Hg loaded on the biochar,  $M_{Hg \text{ out}}$  ( $\mu\text{g}$ ) is the mass of Hg eluted from the biochar,  $M_{\text{biochar}}$  is the mass of biochar in the treatment cell,  $C_{\text{input } i}$  ( $\mu\text{g L}^{-1}$ )

$C_{i-1}$  is the concentration of unfiltered THg in the input solution at week  $i$ ,  $V_{input\ i}$  (L) is the volume of the input solution added to the treatment cell on week  $i$ ,  $C_{output\ i}$  ( $\mu\text{g L}^{-1}$ ) is the concentration of unfiltered THg in the treatment effluent on week  $i$ , and  $V_{output\ i}$  (L) is the volume of treatment effluent collected on week  $i$ . Missing data points were interpolated assuming a linear relationship between two measured points.

### 3.7 Characterization of particles in leachates

Unfiltered samples derived from HMT (weeks 57, 81, and 111), H6S (week 57), THC-HMT (weeks 52 and 82), and THC-H6S (weeks 40 and 50) were characterized using transmission electron microscopy (TEM). TEM samples were prepared by placing 5-10  $\mu\text{L}$  of unfiltered aqueous sample on standard 200 mesh Cu grids (CANEMEC Inc., Montréal, QC, Canada) or on lacey formvar/carbon coated 200 mesh Ni grids (SPi®, SPi Supplies, London, ON, Canada). The prepared samples were analyzed using a Philips CM10 TEM operating at 60 KV at the University of Waterloo to obtain particle size information, with three to nine locations were randomly selected for each sample.

### 3.8 Solid-phase analyses

Solid-phase extractions, including a five-step sequential extraction, total Hg digestion, and MeHg digestion, were conducted on solid samples collected at different depths within the treatment humidity cells at the termination of the experiment. Duplicate extractions were conducted on each solid sample. Quartz sand used in the treatment columns had limited impurity and retention. Therefore, concentrations can be corrected for the biochar mass in each column to represent concentrations retained on the biochar.

A five-step Hg sequential extraction procedure, developed by Bloom et al. (2003), was used to target water soluble (F1; WAT), stomach acid soluble (F2; STO), organo-

chelated (F3; ORG), elemental (F4; ELE), and mercuric sulfide (F5; SUL) fractions using the following extractants: Ar-purged Milli-Q water (WAT), 0.1 M CH<sub>3</sub>COH + 0.1 M HCl at pH 2 (STO), 0.1 M KOH (ORG), 12 M HNO<sub>3</sub> (ELE), and aqua regia (SUL). Concentrations of total Hg retained on the biochar were determined by digesting 0.5 g of solid material in aqua regia for 3 d. Solid-phase concentrations of MeHg were obtained by digesting 0.2 to 2 g of solid material using 20% KCl and 8 M H<sub>2</sub>SO<sub>4</sub> with an addition of 0.2 M CuSO<sub>4</sub> for distillation, with the digestate analyzed using the method described above.

Statistical differences for the solid-phase concentrations on the biochar within each treatment column were determined using single-factor analyses of variance (ANOVA) at a 95% confidence level ( $p < 0.1$ ). Differences for the THg retained on the biochar determined using the sum of Hg extracted at each step from the five-step sequential extraction method and concentrations of Hg obtained from the THg digestion were analyzed using two-factor ANOVA at a 95% confidence level ( $p < 0.1$ ). Significant differences between the means of measured solid-phase concentration on the biochar at different depths within each treatment column were determined using Fisher's least significant difference (LSD) (Montgomery, 2012).

### **3.9 X-ray absorption spectroscopy (XAS)**

#### **3.9.1 Reference materials**

Mercury reference compounds included mineral specimens of cinnabar ( $\alpha$ -HgS) and corderoite (Hg<sub>3</sub>S<sub>2</sub>Cl<sub>2</sub>) (Excalibur Mineral Corp., Peekskill, NY, USA) as well as reagent-grade mercury compounds HgO, HgCl<sub>2</sub>, and HgSO<sub>4</sub> (Sigma-Aldrich, Oakville, ON, Canada). The spectrum of metacinnabar ( $\beta$ -HgS) was obtained from the Hephaestus

utility of the Demeter software package (Ravel and Newville, 2005). Eighteen S reference compounds representing a wide range of oxidation states of S were analyzed (Table A 3). These references included natural mineral specimens, pyrrhotite ( $\text{Fe}_{(1-x)}\text{S}$ ),  $\alpha$ -HgS, pentlandite ( $(\text{Fe,Ni})_9\text{S}_8$ ), pyrite ( $\text{FeS}_2$ ), marcasite ( $\text{FeS}_2$ ), metacinnabar ( $\beta$ -HgS), elemental S ( $\text{S}_8$ ),  $\text{Na}_2\text{SO}_3$ ,  $\text{HgSO}_4$ ,  $\text{FeSO}_4$ ,  $\text{NiSO}_4$ ,  $\text{K}_2\text{SO}_4$ , and gypsum ( $\text{CaSO}_4 \cdot 2\text{H}_2\text{O}$ ) to represent inorganic S compounds. Organic S reference compounds included dibenzyl disulfide, L-cysteine, dibenzo thiophene (Sigma-Aldrich, Oakville, ON, Canada), tetramethylene sulfoxide (Acros Organics, Thermo Fisher Scientific, Burlington, ON, Canada), and sodium methane sulfonate (Alfa Aesar, Fisher Scientific, Ottawa, ON, Canada).

### 3.9.2 Micro X-ray absorption spectroscopy ( $\mu$ -XAS)

Micro X-ray absorption spectroscopy ( $\mu$ -XAS) analyses, including micro X-ray fluorescence ( $\mu$ -XRF) mapping and micro X-ray absorption near edge structure ( $\mu$ -XANES) analysis, were conducted at beamline 13-ID-E at the Argonne National Laboratory, IL, USA. A four-element silicon drift detector (Vortex ME-4, SII Nanotechnology USA Inc., Northridge, CA, USA) and a focused ion beam measuring  $2 \times 2 \mu\text{m}$  were used to collect  $\mu$ -XRF maps of Hg and other elements on the polished thin sections. A bag that was continuously purged with He was placed around the sample stage to minimize radiation damage and reduce absorption by air. The  $\mu$ -XRF maps for Si  $\text{K}\alpha$  and S  $\text{K}\alpha$  fluorescence lines were collected at 2,550 eV, and the  $\mu$ -XRF maps for Fe  $\text{K}\alpha$ , Cu  $\text{K}\alpha$ , and Hg  $\text{L}\alpha$  fluorescence lines were collected at 13,000 eV. Spots with elevated intensities of Hg were selected to collect  $\mu$ -XANES across the S K-edge at 2,472 eV and across the Hg  $\text{L}_{\text{III}}$ -edge at 12,284 eV.

### 3.9.3 X-ray absorption near edge structure (XANES)

Sulfur K-edge XANES spectra for bulk biochar samples and reference materials were collected at the Soft X-ray Microcharacterization Beamline (SXRMB) at the Canadian Light Source (CLS, Saskatoon, SK, Canada) using a Si (111) monochromator. A broad beam, measuring 3 × 2 mm, was used to collect spectra in fluorescence mode. Unused biochar and biochar collected at the termination of the experiments were analyzed. The biochar samples and the reference materials were homogenized and smeared as thin films on conductive double-sided tape on a copper sample holder. The sample holder was then mounted in a chamber under vacuum during the analyses. Three scans were collected for each sample, and the scans merged before normalization.

Mercury L<sub>III</sub>-edge XANES spectra for the floodplain soil (MOTO) and the riverbank sediment (SR6) were collected on beamline 20-ID-B,C-PNC/XSD at the Advanced Photon Source (Argonne National Laboratory, Lemont, IL, USA) using a 4-element Si drift detector (Vortex<sup>®</sup>, Hitachi High-Technologies Science America Inc., Chatsworth, CA, USA) in fluorescence mode. A defocused beam measuring 500 × 1,000 μm were used.

### 3.9.4 Spectra analyses

Data processing for μ-XANES spectra and XANES spectra were performed using ATHENA (Ravel and Newville, 2005). Linear combination fitting analyses were conducted following the “Combo method” described by Manceau et al. (2012). Sulfur K-edge μ-XANES spectra and XANES spectra were also decomposed into several Gaussian peaks between 2,466 and 2,489 eV following Manceau and Nagy (2012). Two arctangent steps, representing reduced S species (2,474 eV) and oxidized S species

(2,482.5 eV), were used to decompose spectra for reference compounds and the biochar samples. The collected spectra for reference compounds were first decomposed into Gaussian peaks to determine the whiteness positions indicative of different S species (Figures A 2-4). Ten Gaussian peaks (Table A 4), representing sulfide minerals (2470.4, 2471.5, and 2472.3 eV), exocyclic S (2473.5 eV), heterocyclic S (2474 eV), sulfoxide (2476.1 eV), sulfite (2478.5 eV), sulfone (2480.2 eV), sulfonate (2481.4 eV), and sulfate (2482.7 eV), were used to decompose S K-edge  $\mu$ -XANES spectra and XANES spectra for the biochar samples by constraining peak widths within a range of 0.65 to 0.8. Fitting qualities were estimated using a normalized-square sum (NSS) method described by Manceau and Nagy (2012):

$$NSS = \sum (fit - normalized)^2 / \sum normalized^2.$$

The area under a Gaussian peak for a given S species is proportional to the number of vacancies in 3p transitions, and thus increases with oxidation state (Waldo et al., 1991). Scaling factors (Figure A 5; Table A 4), estimated by normalizing the area under each Gaussian peak to the area under the Gaussian peak of elemental S at 2,472 eV, were used to account for the changes in absorption cross section and quantify fractions in each species following Manceau and Nagy (2012).

## 4 Results and Discussion

### 4.1 Overview of riverbank sediment and floodplain soil

Both SR6 and MOTO are abundant in Al, Fe, soil organic matter, and clay minerals with relatively low S contents (<400  $\mu\text{g g}^{-1}$ ) (Table A 1). SR6 and MOTO are fine-grained and

classified as silty loam based on the USDA soil texture triangle (Soil Survey Division Staff., 1993). Hg L<sub>III</sub>-edge X-ray absorption near edge structure (XANES) analyses revealed that Hg is mainly present as metacinnabar ( $\beta$ -HgS), cinnabar ( $\alpha$ -HgS) and Hg sorbed on goethite (Figure A 6).

## 4.2 Overview of hardwood biochar

Characterization of the hardwood biochar was conducted in previous studies (Liu et al., 2015, 2018). The hardwood biochar mainly contained C (99.9%) with lesser amounts of Ca (2,900  $\mu\text{g g}^{-1}$ ) and K (2,600  $\mu\text{g g}^{-1}$ ). The surface area of the hardwood biochar is 65  $\text{m}^2 \text{g}^{-1}$ . The most abundant functional groups on the hardwood biochar were hydroxyl, aliphatic, and carboxylic groups.

## 4.3 Chemical composition of input solutions

Leachates derived from humidity cells containing floodplain soil (HMT) and riverbank sediment (H6S) had varying composition over the 100-week duration of the experiment (Table 1). Leachates derived from HMT and H6S had generally consistent concentrations of DOC, dissolved anions ( $\text{Cl}^-$ ,  $\text{NO}_3^-$ ,  $\text{SO}_4^{2-}$ ), major cations (Na, Mg, Si, and K), and other trace elements with minor fluctuations. Slightly different values for pH, alkalinity, and concentrations of Al and Ca were observed for the leachates derived from HMT and H6S, mainly due to the different input solutions used for these source columns (Table 1). Results of TEM analyses indicate that leachate derived from HMT and H6S contained aggregates of nano-scale particles (Figure A 7), which is consistent with the mobilization of Hg through the release of colloidal particles from flooded riverine soil (Hofacker et al., 2013; Lowry et al., 2004; Poulin et al., 2016).

The unfiltered leachates derived from HMT and H6S contained elevated concentrations of THg that varied over the duration of the experiment (Figure 2). Effluent concentrations of unfiltered THg derived from HMT ranged from 11,800 to 55,300 ng L<sup>-1</sup> over the 100-week experimental period. Unfiltered effluent concentrations of THg derived from H6S varied from 1,500 to 14,600 ng L<sup>-1</sup> with a mean value of 4,600 ng L<sup>-1</sup> from weeks 1 to 63, before rapidly increasing to 36,800 ng L<sup>-1</sup> at week 84 and then dropping to 6,160 ng L<sup>-1</sup> at week 92. The relatively large variations in the chemical composition of leachates from HMT and H6S are attributed to the weekly application of simulated acidic rain water (ARW), river water (SRW) which induce oscillations in pore water chemistry and affect kinetic release rates. These variations are consistent with leachate chemistry derived from other humidity cell experiments (e.g., Ardaou et al., 2009; Langman et al., 2015a, 2015b; Maest and Nordstrom, 2017). Concentrations of unfiltered THg from HMT and H6S are similar to the release of total Hg under saturated flow conditions (Desrochers, 2013, 2015; Paulson, 2014; Paulson et al., 2016) and saturated static conditions (Liu et al., 2017) for sediments collected near South River, VA, USA, whereas the release of total Hg under saturated flow and static conditions mostly occurred in the fraction passing a 0.45- $\mu$ m filter.

Concentrations of 0.45- $\mu$ m filtered THg and from HMT ranged from 1,520 to 9,010 ng L<sup>-1</sup>, with a maximum occurring at week 43. Concentrations of 0.45- $\mu$ m filtered THg from H6S fluctuated less, ranging from 322 to 741 ng L<sup>-1</sup> over the course of the experiment. The relatively low proportions of 0.45- $\mu$ m to unfiltered THg in HMT and H6S suggest that the majority of Hg release under flooding and drainage conditions was

present in particulate forms, whereas Hg release under saturated flow/static conditions was present in dissolved (or colloidal) forms.

#### 4.4 Composition of effluent from treatment columns

Passage of the source column (HMT and H6S) effluent through the biochar columns, designed to represent a reactive mat, resulted in limited changes in aqueous chemical composition (Table 1; Figures A 8-9). Concentrations of DOC ( $< 10 \text{ mg L}^{-1}$ ), organic acids ( $< 0.5 \text{ mg L}^{-1}$ ),  $\text{NO}_3^-$  ( $< 10 \text{ mg L}^{-1}$ ), and Ca in the treated effluent were close to the effluent from the respective source columns. Concentrations of  $\text{SO}_4^{2-}$ , Mg, and K in the treated effluent were slightly higher than in effluent from the source columns. Lower concentrations of Al and Si were observed in the treated effluent, suggesting removal of these constituents through uptake of clay particles within the porous biochar structure. Application of the hardwood biochar resulted in limited release of  $\text{NH}_3\text{-N}$  ( $< 0.3 \text{ mg L}^{-1}$ ) and  $\text{PO}_4\text{-P}$  ( $< 2 \text{ mg L}^{-1}$ ).

Application of the hardwood biochar resulted in lower concentrations of both unfiltered and  $0.45\text{-}\mu\text{m}$  filtered THg in the treatment effluent derived from the treatment columns (THC-HMT and THC-H6S) than from the source columns (HMT and H6S) (Figure 2). The weekly removal varied over the duration of the experiment and is attributed to the variable Hg release from the source columns. Concentrations of unfiltered THg derived from THC-HMT varied from a minimum of  $1,440 \text{ ng L}^{-1}$  at week 23 to a maximum of  $35,100 \text{ ng L}^{-1}$  at week 25, while concentrations of  $0.45\text{-}\mu\text{m}$  filtered THg varied from a minimum of  $95 \text{ ng L}^{-1}$  at week 23 to a maximum of  $2,530 \text{ ng L}^{-1}$  at week 25. Weekly Hg removal by THC-HMT ranged from 19 to 90% (unfiltered) and 50 to 90% ( $0.45\text{-}\mu\text{m}$  filtered). The minimum THg removal for both unfiltered and  $0.45\text{-}\mu\text{m}$

filtered THg occurred at week 25 when the lowest Hg release from HMT occurred.

Concentrations of unfiltered THg derived from THC-H6S varied from a minimum of 121 ng L<sup>-1</sup> at week 19 to a maximum of 1,230 ng L<sup>-1</sup> at week 40, while concentrations of 0.45- $\mu$ m filtered THg varied from a minimum of 44 ng L<sup>-1</sup> at week 16 to a maximum of 422 ng L<sup>-1</sup> at week 75. Weekly Hg removal values in THC-H6S were > 90% (unfiltered) and > 66% (0.45- $\mu$ m filtered).

Concentrations of total Hg retained in the biochar were estimated by normalizing differences between concentrations of unfiltered THg in the source and the treatment effluents to the mass of biochar in the treatment columns. Mercury retained in the THC-HMT biochar was twice as the concentration retained in THC-H6S (Table 2), with this difference likely related to the relatively higher release of Hg from HMT (Table 1). The estimated total mass of Hg retained in the biochar represents > 80% Hg removal by the THC-HMT column and > 96% removal by the THC-H6S column (Table 2).

The MeHg concentrations in treatment effluents were lower than those derived from the source columns (Table 1). Minor formation of MeHg in treatment effluents was observed for THC-HMT (< 1.0 ng L<sup>-1</sup>) and THC-H6S (< 0.5 ng L<sup>-1</sup>) (Figure 3).

#### 4.5 Solid-phase extractions

Concentrations of Hg retained on the biochar collected at the termination of the experiment show different distributions within the two treatment columns (Figure 4). No significant differences were observed between two methods (the sum of Hg extracted from the five-step sequential extraction and the *aqua regia* digestion) used to determine total Hg retained on the biochar. Total Hg retained in biochar at different depths changed significantly ( $p < 0.002$ ) for THC-HMT and THC-H6S. Mercury retained on the

biochar collected from THC-HMT, which had a higher concentration of unfiltered THg in the input, was present throughout the entire column length with minor differences.

Mercury retained on the biochar collected from THC-H6S, which had a lower concentration of unfiltered THg in the input, was mainly distributed close to the air/biochar-sand interface (0-2 cm), with concentrations then decreasing with increasing depth.

Different concentrations of Hg retained in the biochar in THC-HMT and THC-H6S could be related to the differences in Hg loading to the treatment columns. The lower mass of Hg retained in the biochar in THC-H6S is likely related to lower Hg release from H6S than from HMT. Lower Hg removal observed in THC-HMT than in THC-H6S (Figure 1, Table 2) could also be attributed to the relatively acidic pH values and alkalinity (Table 1) derived from HMT.

Results of Hg extraction on the biochar collected from THC-HMT and THC-H6S (Figure 4) at the end of the experiment indicate the hardwood biochar had not reached its removal capacity for stabilizing Hg-bearing particles after 100 weeks (82 pore volumes for THC-HMT and 101 pore volumes for THC-H6S), especially for THC-H6S that had 30% of the Hg loading of THC-HMT. The decrease in Hg in the biochar at greater depth in THC-H6S suggests that Hg first accumulated near the air/biochar-sand interface (0-2 cm) at the beginning of the experiment until the removal capacity of biochar at this location was exceeded. Over time, Hg had penetrated further and accumulated at greater depths. The accumulation of the majority of Hg at 0-2 cm in THC-H6S is consistent with a previous study where the majority of Hg was observed to

accumulate within the first 2 cm when the same hardwood biochar was used to stabilize Hg derived from river bank sediments under saturated flow conditions (Paulson., 2014).

Results of the five-step sequential extraction procedure indicate that Hg retained in the biochar was mainly present in the organic-chelated Hg (ORG), and elemental Hg (ELE) fractions (Figure 4), with minimal amounts of water soluble Hg (WAT), weak acid extractable Hg (STO), and mercury sulfide and residual forms (SUL). For the biochar in THC-HMT, concentrations of Hg extracted from the ELE, and SUL fractions were significantly lower ( $p < 0.004$ ) at depths of 0-2 and 6-8 cm than from 2-6 cm, whereas variations in the concentrations of Hg extracted from the ORG fraction were not significantly over the length of the column ( $p > 0.01$ ). For the biochar in THC-H6S, concentrations of Hg extracted from the ORG, ELE, and SUL fractions decreased significantly ( $p < 0.02$ ) from 0-2 cm to greater depths (Figure 4). As the total Hg retained on the biochar in THC-H6S decreased, Hg on the biochar shifted from the ELE fractions towards to the ORG fractions. Percentage of Hg extracted from the ELE fraction decreased from 49 to 26%, whereas percent of Hg extracted from the ORG fraction increased from 46 to 66%. This shift in relative percentage of Hg extracted from the ELE towards ORG fractions as loading concentration decrease indicates Hg tends to bound to functional groups on biochar at lower concentrations.

The minimal presence of WAT and STO fractions for biochar in THC-HMT and THC-H6S suggest Hg retained on the biochar is present in less mobile forms. This observation is consistent with a study in which hardwood biochar was used as a reactive mat under saturated flow conditions (Paulson, 2014). In the same study, no

significant release of Hg occurred when the biochar was exposed to SRW, and minimal release when it was exposed to ARW (Paulson, 2014).

Insoluble and fine-grained HgS phases with impurities, such as Fe and Zn, can be extracted in the ELE fraction when the total Hg concentration is less than  $20 \mu\text{g g}^{-1}$  (Bloom et al., 2003; Kim et al., 2003). The floodplain soil mainly contains  $\beta$ -HgS (Figure A 6), likely in nanoparticulate form (Figure A 7) and associated with other metals, suggesting Hg extracted in the ELE step might also have targeted HgS phases.

Results for MeHg on the biochar suggest a minimal presence ( $< 0.02 \text{ ng g}^{-1}$ ) in solid samples collected at the termination of the experiment, with the distribution (Figure 5) following a similar pattern to the total Hg distribution (Figure 4). Changes in biochar MeHg concentrations in THC-HMT were insignificant with an overall mean of  $0.15 \pm 0.02 \text{ ng g}^{-1}$ . MeHg in biochar in THC-H6S decreased significantly ( $p = 0.037$ ) from the air/biochar-sand interface ( $0.10 \pm 0.04 \text{ ng g}^{-1}$ ) to greater depths ( $0.01 \pm 0.01 \text{ ng g}^{-1}$ ). The concentrations of MeHg on the biochar represented less than 0.01% of total Hg retained on the biochar. The concentrations of MeHg on biochar from THC-HMT and THC-H6S are similar to those in a study that used the same hardwood biochar for Hg removal under aerobic fully-saturated flow conditions (Paulson, 2014), and the concentrations were more than 100 times lower than those observed in a study of Hg removal in anoxic sediments using the hardwood biochar (Liu et al., 2018). The relatively low concentrations of solid-phase MeHg in biochar collected at the end of the experiment suggest the hardwood biochar might be a good candidate as a reactive material installed under flooding and drainage conditions without promoting MeHg production.

#### 4.6 Synchrotron X-ray absorption spectroscopy analyses

Micro XRF maps were collected on polished thin sections prepared with hardwood biochar from the air/biochar-sand interface (0-2 cm) of the treatment columns at the termination of the experiment. Results of  $\mu$ -XRF maps for THC-HMT indicate the presence of Si, Fe, S, Cu, and Hg within the porous structure of the biochar (Figure 6). Mercury retained on the biochar co-occurred with S and Cu in isolated locations. Limited Hg hot spots were observed in  $\mu$ -XRF maps collected for biochar from THC-H6S; however, the concentrations of total Hg retained were close to those from THC-HMT, which might be related to the heterogeneous distribution of Hg on the biochar.

Micro-XANES analyses across the Hg L<sub>III</sub>-edge and S K-edge were performed at locations where greater abundances of Hg and S were observed. Results from the Hg L<sub>III</sub>-edge  $\mu$ -XANES results (Figure 7) suggest Hg on the biochar is present in different forms, with linear combination fitting results in derivative mode indicating a composition of ~50% metacinnabar ( $\beta$ -HgS), 43% Hg sorbed on goethite, and 7% HgO. Linear combination fitting was conducted with/without HgO. Excluding HgO (reduced  $X^2 = 1.7 \times 10^{-5}$ ; NSS =  $4.4 \times 10^{-2}$ ) resulted in a fit that did not closely correspond to the normalized spectra. Including HgO (reduced  $X^2 = 8.4 \times 10^{-6}$ ; NSS =  $2.3 \times 10^{-2}$ ) resulted in improved fit to the normalized spectra. This result suggests that HgO was likely a contributing phase for Hg retention by the biochar. A similar composition of Hg phases retained on the biochar was identified at a second location for the biochar collected at 0-2 cm in THC-HMT. Metacinnabar and Hg sorbed on iron oxides (Figure A 6) have been observed in the same floodplain soil sample obtained from the South River, Virginia, USA which are consistent with common Hg phases observed in sediments at sites contaminated by industrial activities (Gibson et al., 2015; Kim et al., 2000; Lowry et al.,

2004; Poulin et al., 2016; Rimondi et al., 2014; Santoro et al., 2010; Terzano et al., 2010). The presence of  $\beta$ -HgS and Hg sorbed on iron oxides on biochar suggest retention of particles derived from floodplain soil.

The differences between the Hg sequential extraction analyses and linear combination fitting of Hg L<sub>III</sub> edge  $\mu$ -XANES spectra from the biochar can be related to differences between these two techniques. Sequential Hg extraction method targets different phases of Hg in bulk samples of biochar, whereas Hg L<sub>III</sub>-edge  $\mu$ -XANES analyses directly indicate chemical speciation of Hg in a 2  $\mu$ m  $\times$  2  $\mu$ m beam size area where the spectra were collected (Figure 7)..

Sulfur K-edge  $\mu$ -XANES spectra collected at the same locations where Hg L<sub>III</sub>-edge  $\mu$ -XANES were collected show peaks at 2470.4, 2473.5, and 2482.7 eV (Figure A 10). The results of Gaussian peak fitting suggest the spectra are mainly composed of sulfide, exocyclic S, and sulfate. The presence of these groups is consistent with observations by Cheah et al. (2014) for XANES spectra collected on biochar prepared with oak or corn stover. Minimal amounts of other S phases, such as sulfoxide, sulfite, sulfone, and sulfonate, might also be present at the location where S K-edge  $\mu$ -XANES spectra were collected (Figure A 10). Sulfur groups, including sulfide, elemental S, exocyclic S, heterocyclic S, sulfoxide, sulfone, sulfonate, and sulfate, are common in soil containing natural organic matter (Prietz et al., 2003; Manceau and Nagy, 2012). The S groups identified by  $\mu$ -XANES analyses might have originated from S phases present in the floodplain soil.

Three main peaks at 2,473.5, 2,476.1, and 2,482.7 eV were observed on the S K-edge XANES spectra for the unused biochar (Figure 8), and these correspond to

exocyclic S functionalities, sulfoxide, and sulfate or ester S functionalities (Table A 4) (Cheah et al., 2014; Manceau and Nagy, 2012). The peak at 2,476.1 eV is less pronounced for the biochar collected at different depths from the treatment columns, indicating a loss of sulfoxide functional groups. Wider peak shoulders are observed at approximately 2,470.4 and 2,472.3 eV for the biochar after treatment relative to the unused biochar, suggesting accumulations of sulfide minerals during treatment (Figure 8).

Results of Gaussian peak fitting and linear combination fitting both suggest decreases in fractions of reduced S functionalities and sulfoxide for the biochar in THC-HMT and THC-H6S at the termination of the experiment than for the unused biochar (Figures 8b-d and 9; Table A 5). The decrease in the fraction of reduced S functionalities can be related to the formation of Hg-thiol complexes on the biochar (Liu et al., 2016). The disappearance of the sulfoxide peak for biochar collected at 0-2 cm (Figure 8) and the decrease in sulfoxide fractions for the biochar collected at greater depths in THC-HMT and THC-H6S (Figure 9) can be related to the formation of Hg-O complexes on biochar with sulfoxide functional groups. Sulfoxide has the potential to form O-bonded complexes with various metals, such as Fe, Cu, or Hg (Calligaris and Carugo, 1996; Calligaris, 2004). For example, the use of dimethyl sulfoxide to pre-treat *Aspergillus flavus* biomass improved the biosorption of Pb (II) and Cu (II) from aqueous solution (Akar and Tunali, 2006). An EXAFS study indicates Hg tends to form complexes with sulfoxide as six Hg-O bonds (Persson et al., 2008). Fractions of sulfoxide on the biochar are not statistically correlated with the total Hg retained on the biochar, which could be related to competition between Hg and other metals present in

input solutions derived from HMT and H<sub>6</sub>S, such as Fe or Mn (Table 1) as well as Hg forming complexes with other functional groups on the biochar as suggested by the five-step sequential extraction method (Figure 4).

Results of Gaussian peak fitting and linear combination fitting also both suggest increases in the fractions of sulfide and intermediate S (sulfone and sulfonate) for the biochar in THC-HMT and THC-H<sub>6</sub>S at the termination of the experiment than for the unused biochar (Figures 8b-d and 9; Table A 5). The increase in the sulfide fraction is consistent with the accumulation of Hg-S on the biochar as suggested by the five-step sequential extractions (Figure 4),  $\mu$ -XRF maps, Hg L<sub>III</sub>-edge  $\mu$ -XANES (Figures 6-7), and S K-edge  $\mu$ -XANES (Figure A10). Formation of H-S from aggregation of Hg-thiolate occurs in the presence of organic matter (Manceau et al., 2015). The increase in sulfide fractions, coupled with decreases in reduced S fractions, in the biochar is also likely related to the formation of Hg-S through aggregation of Hg-thiolate complexes. The increase in intermediate S species within the biochar after treatment is consistent with the results of S K-edge  $\mu$ -XANES (Figure A10). The increases in both sulfide and intermediate S fractions may be related to the accumulation of particles derived from the floodplain soil.

#### **4.7 Long-term performance of the hardwood biochar**

The results of this study can be used to assess whether hardwood biochar can be used to promote sustained removal of Hg when installed in a riverine environment. Under the rapid drainage conditions and short residence times (<5 h) used in this experiment, the hardwood biochar stabilized >80% Hg derived from source columns over a 100-week duration. These results suggest that the hardwood biochar may be a highly effective

material for long-term use as reactive mat under environmentally relevant flooding and drainage conditions.

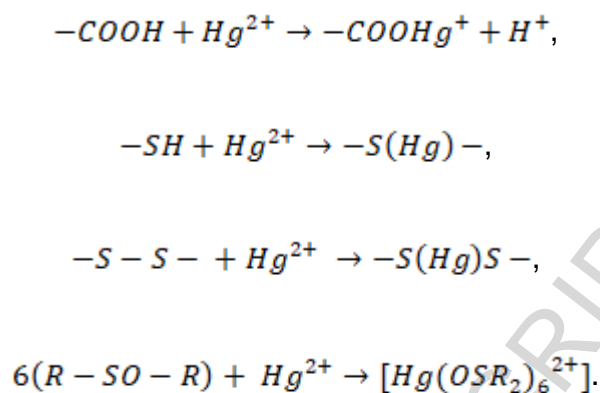
Previous studies have shown that information extracted from laboratory-scale humidity cell experiments can provide a reasonable assessment of solute release and microbial processes for medium-scale (> 1,000 kg and < 10,000 kg) field studies (Langman et al., 2015a, 2015b; Maest and Nordstrom, 2017; Wilson et al., 2018). A similar prediction using humidity cell data is not available for Hg release under field conditions. Variations in local geochemical properties, changes in seasonal temperatures and hydrographic conditions may limit direct transfer of humidity cell predictions. For example, extreme storm events associated with climate change can lead to dramatic increases in the release of Hg to aquatic environments (Krabbenhoft and Sunderland 2013), which may not be captured in laboratory testing. Therefore, field pilot studies are recommended before implementing large-scale engineered remediation projects using biochar for Hg stabilization.

#### **4.8 Proposed mechanisms for Hg removal**

The mechanisms involved in Hg stabilization using hardwood biochar under conditions representative of typical fluvial settings can be attributed to a combination of physicochemical processes, including the formation of complexes with functional groups on the biochar surfaces and the retention/filtration of particulate Hg within the biochar porous structure.

Mercury can form complexes with functional groups on the biochar surface, including carboxylic groups, thiol functionalities, and sulfoxide groups (Calligaris, 2004;

Calligaris and Carugo, 1996; Liu et al., 2017, 2016; Persson et al., 2008; Uchimiya et al., 2012) via reactions including:



Carboxyl groups are one of the most abundant functional groups in the biochar (Liu et al. 2015), which are known to promote the removal of heavy metals in contaminated sediment (Uchimiya et al., 2012). Concentrations of Hg extracted from the ORG fraction for biochar in THC-HMT and THC-H6S (Figure 4) may represent the release of Hg bound to carboxyl groups. Other functional groups, including sulfoxide and thiol, can also contribute to the removal of Hg. Results of S K-edge XANES for biochar in THC-HMT and THC-H6S (Figures 8-9) and  $\mu$ -XANES for selected locations on biochar at depth 0-2 cm (Figure A 10) indicate a decrease in peak intensity at 2,476.1 eV compared to the spectra for the unused biochar, suggesting the formation of metal-sulfoxide complexes (Calligaris, 2004; Calligaris and Carugo, 1996; Persson et al., 2008). A decrease in reduced S functionalities with depth suggested by S K-edge XANES for the biochar in THC-HMT and THC-H6S (Figure 9) may be related to the formation of metal and thiol functional complexes, as suggested in studies of Hg removal from aqueous solution using the same type of biochar (Liu et al., 2016) and from riverbank sediment under strongly reducing conditions (Liu et al., 2017).

Particles derived from the floodplain soil were also retained within the biochar porous structure. Results of  $\mu$ -XRF for the biochar collected from the air/biochar-sand interface (0-2 cm) indicate a visual correlation between Hg and S, and the presence of other metals and clay minerals within the porous structure (Figure 6). Results from sequential extraction (Figure 4) and Hg L<sub>III</sub>-edge  $\mu$ -XANES (Figure 7) analyses suggest the presence of Hg-S phases in the biochar collected from the treatment columns, which might be related to the retention of metacinnabar ( $\beta$ -HgS) (Figure 7) and other sulfide minerals as observed in the results of S K-edge  $\mu$ -XANES (Figure A 10) and S K-edge XANES (Figures 8-9) analyses of floodplain soil (Figure A 6).

The relative contributions of physicochemical processes controlling Hg removal appear to differ depending on the extent of Hg loading. At low loading, Hg is primarily bound to surface functional groups on the biochar. As loading increases, other metals derived from natural sediment, including Fe and Cu, compete with Hg for available sites on the biochar surface. At higher loading, when limited functionalities are available, the physical filtration of particulate-bound Hg-S phases and other metal-bearing phases becomes the dominant removal mechanism.

## 5 Conclusions

This study indicates that biochar prepared from hardwood can minimize the release and transport of particulate and dissolved Hg derived from riverbank sediments under the rapid drainage flow conditions and short residence times representative of dynamic fluvial systems. Relatively low concentrations of MeHg observed in effluent from treatment columns and in solid material at the end of the experiment suggest the

application of biochar does not promote methylation reactions. Relatively low concentrations of other dissolved constituents suggest that application of the hardwood biochar does not release undesirable constituents (e.g., N, P), thus minimizing the potential for unintended environmental consequences. The application of the hardwood biochar in flow-through systems, such as reactive mats, has the potential for controlling long-term Hg release and transport in fluvial settings characterized by frequent changes in hydrological and geochemical conditions.

## 6 Acknowledgements

Funding for this research was provided by the Natural Sciences and Engineering Research Council of Canada (NSERC), E. I. du Pont de Nemours and Company Canada, and an Ontario Research Fund (ORF) Research Excellence grant. TEM analyses were performed at the Canadian Centre for Electron Microscopy at McMaster University, which is supported by NSERC and other government agencies. Micro X-ray absorption spectroscopy ( $\mu$ -XAS) analyses were performed at GeoSoilEnviroCARS (The University of Chicago, Sector 13), Advanced Photon Source (APS), Argonne National Laboratory. GeoSoilEnviroCARS is supported by the National Science Foundation - Earth Sciences (EAR - 1634415) and Department of Energy - GeoSciences (DE-FG02-94ER14466). Bulk Hg L<sub>III</sub>-edge X-ray absorption spectroscopy (XAS) for riverbank sediment and floodplain soils was conducted on beamline 20-ID-B, C- PNC/XSD, Advanced Photon Source, Argonne National Laboratory. Sector 20 operations are supported by the US Department of Energy and the Canadian Light Source. This research used resources of the Advanced Photon Source, an Office of

Science User Facility operated for the U.S. Department of Energy (DOE) Office of Science by Argonne National Laboratory and was supported by the U.S. DOE under Contract No. DE-AC02-06CH11357 and the Canadian Light Source and its funding partners. Sulfur K-edge X-ray absorption spectroscopy (XAS) analyses were performed at the Canadian Light Source, which is supported by the Canada Foundation for Innovation, NSERC, the University of Saskatchewan, the Government of Saskatchewan, Western Economic Diversification Canada, the National Research Council Canada, and the Canadian Institutes of Health Research. We are grateful for advice and assistance from K. Elena, S. Fellin, P. Liu, J. Hu, and L. Groza with respect to analytical sampling and chemical analyses. We are also thankful for the advice and contributions of the South River Science Team.

## 7 References

- Akar, T., Tunali, S., 2006. Biosorption characteristics of *Aspergillus flavus* biomass for removal of Pb(II) and Cu(II) ions from an aqueous solution. *Bioresour. Technol.* 97, 1780–1787. doi:10.1016/j.biortech.2005.09.009
- APHA, 2005. Standard Method for Examination of Water and Waste Water, 21st ed.
- Ardau, C., Blowes, D.W., Ptacek, C.J., 2009. Comparison of laboratory testing protocols to field observations of the weathering of sulfide-bearing mine tailings. *J. Geochemical Explor.* 100, 182–191. doi:10.1016/j.gexplo.2008.06.005
- ASTM, 2012. Standard D5744-12: Standard Test Method for Laboratory Weathering of Solid Materials Using a Humidity Cell, 1–19. doi:10.1520/D5744-12.2
- Babiarz, C., Hoffmann, S., Wieben, A., Hurley, J., Andren, A., Shafer, M., Armstrong, D., 2012. Watershed and discharge influences on the phase distribution and tributary loading of total mercury and methylmercury into Lake Superior. *Environ. Pollut.* 161, 299–310. doi:10.1016/j.envpol.2011.09.026
- Bloom, N.S., Preus, E., Katon, J., Hiltner, M., 2003. Selective extractions to assess the biogeochemically relevant fractionation of inorganic mercury in sediments and soils. *Anal. Chim. Acta* 479, 233–248. doi:10.1016/S0003-2670(02)01550-7
- Bundschuh, M., Zubrod, J.P., Seitz, F., Newman, M.C., 2015. Effects of two sorbents applied to mercury-contaminated river sediments on bioaccumulation in and detrital processing by *Hyalella Azteca*. *J. Soil. Sediments.* 15, 1265-1274. doi: 10.1007/s11368-015-1100-z
- Calligaris, M., 2004. Structure and bonding in metal sulfoxide complexes: An update. *Coord. Chem. Rev.* 248, 351–375. doi:10.1016/j.ccr.2004.02.005
- Calligaris, M., Carugo, O., 1996. Structure and bonding in metal sulfoxide complexes. *Coord. Chem. Rev.* 153, 83–154. doi: 10.1016/0010-8545(95)01193-5.
- Carter, L.J., 1977. Chemical plants leave unexpected legacy for two Virginia rivers. *Science* 198, 1015–1020. doi:10.1126/science.198.4321.1015
- Cheah, S., Malone, S.C., Feik, C.J., 2014. Speciation of sulfur in biochar produced from pyrolysis and gasification of oak and corn stover. *Environ. Sci. Technol.* 48, 8474–8480. doi:10.1021/es500073r
- Desrochers, K.A., 2013. Geochemical characterization and assessment of stabilization mechanisms for mercury contaminated riverbank sediments from the South River, Virginia (USA). MSc Thesis, Earth Sciences, University of Waterloo, Waterloo, ON, Canada.
- Desrochers, K.A.N., Paulson, K.M.A., Ptacek, C.J., Blowes, D.W., Gould, W.D., 2015. Effect of electron donor to sulfate ratio on mercury methylation in floodplain sediments under saturated flow conditions. *Geomicrobiol. J.* 32, 924–933. doi:10.1080/01490451.2015.1035818
- Eggleston, J., 2009. Mercury loads in the South River and simulation of mercury total maximum daily loads (TMDLs) for the South River, South Fork Shenandoah River, and Shenandoah River: Shenandoah Valley, Virginia Scientific Investigations Report 2009 – 5076, Virginia and Department of Environmental Quality U.S. Environmental Protection Agency.

- Flanders, J.R., Turner, R.R., Morrison, T., Jensen, R., Pizzuto, J.E., Skalak, K., Stahl, R., 2010. Distribution, behavior, and transport of inorganic and methylmercury in a high gradient stream. *Appl. Geochem.* 25, 1756–1769. doi:10.1016/j.apgeochem.2010.09.004
- Gibson, B.D., Ptacek, C.J., Blowes, D.W., Daugherty, S.D., 2015. Sediment resuspension under variable geochemical conditions and implications for contaminant release. *J. Soils Sediments.* 15, 1644-1656. doi:10.1007/s11368-015-1106-6
- Gilmour, C.C., Podar, M., Bullock, A.L., Graham, A.M., Brown, S.D., Somenahally, A.C., Johs, A., Hurt, R.A., Bailey, K.L., Elias, D.A., 2013a. Mercury methylation by novel microorganisms from new environments. *Environ. Sci. Technol.* 47, 11810–11820. doi:10.1021/es403075t
- Gilmour, C.C., Riedel, G.S., Riedel, G., Kwon, S., Landis, R., Brown, S.S., Menzie, C.A., Ghosh, U., 2013b. Activated carbon mitigates mercury and methylmercury bioavailability in contaminated sediments. *Environ. Sci. Technol.* 47, 13001–13010. doi:10.1021/es4021074
- Gilmour, C.C., Bell, T., Soren A., Riedel, G., Kopec, D., Bodaly, D., Ghosh, U., 2018. Activated carbon thin-layer placement as an *in situ* mercury remediation tool in a Penobscot River salt marsh. *Sci. Total. Environ.* 621, 839-848. doi:10.1016/j.scitotenv.2017.11.050
- Gomez-Eyles, J.L., Yupanqui, C., Beckingham, B., Riedel, G., Gilmour, C., Ghosh, U., 2013. Evaluation of biochars and activated carbons for in situ remediation of sediments impacted with organics, mercury, and methylmercury. *Environ. Sci. Technol.* 47, 13721-13729. doi : 10.1021/es403712q
- Guedron, S., Cossa, D., Grimaldi, M., Charlet, L., 2011. Methylmercury in tailings ponds of Amazonian gold mines (French Guiana): Field observations and an experimental flocculation method for in situ remediation. *Appl. Geochemistry* 26, 222–229. doi:10.1016/j.apgeochem.2010.11.022
- Hofacker, A.F., Voegelin, A., Kaegi, R., Kretzschmar, R., 2013. Mercury mobilization in a flooded soil by incorporation into metallic copper and metal sulfide nanoparticles. *Environ. Sci. Technol.* 47, 7739–7746. doi:10.1021/es4010976
- Hu, H.Y., Lin, H., Zheng, W., Tomanicek, S.J., Johs, A., Feng, X.B., Elias, D.A., Liang, L.Y., Gu, B.H., 2013. Oxidation and methylation of dissolved elemental mercury by anaerobic bacteria. *Nat. Geosci.* 6, 751–754. doi:10.1038/ngeo1894
- Ippolito, J.A., Strawn, D.G., Scheckel, K.G., Novak, J.M., Ahmedna, M., Niandou, M.A.S., 2012. Macroscopic and molecular investigations of copper sorption by a steam-activated biochar. *J. Environ. Qual.* 41, 1150. doi:10.2134/jeq2011.0113
- Johnson, N.W., Reible, D.D., Katz, L.E., 2010. Biogeochemical changes and mercury methylation beneath an in-situ sediment cap. *Environ. Sci. Technol.* 44, 7280–7286. doi:10.1021/es100161p
- Kim, C.S., Bloom, N.S., Rytuba, J.J., Brown, G.E., 2003. Mercury speciation by X-ray absorption fine structure spectroscopy and sequential chemical extractions: A comparison of speciation methods. *Environ. Sci. Technol.* 37, 5102–5108. doi:10.1021/es0341485
- Kim, C.S., Brown, G.E., Rytuba, J.J., 2000. Characterization and speciation of mercury-bearing mine wastes using X-ray absorption spectroscopy. *Sci. Total Environ.* 261,

- 157–168. doi :10.1016/S0048-9697(00)00640-9
- Kocman, D., Horvat, M., Pirrone, N., Cinnirella, S., 2013. Contribution of contaminated sites to the global mercury budget. *Environ. Res.* 125, 160–170. doi:10.1016/j.envres.2012.12.011
- Krabbenhoft, D., Sunderland, E.M., 2013. Global change and mercury. *Science*. 341 (6153), 1457-1458. doi: 10.1126/science.1242838
- Langman, J.B., Blowes, D.W., Sinclair, S.A., Krentz, A., Amos, R.T., Smith, L.J.D., Pham, H.N., Segó, D.C., Smith, L., 2015a. Early evolution of weathering and sulfide depletion of a low-sulfur, granitic, waste rock in an Arctic climate: A laboratory and field site comparison. *J. Geochemical Explor.* 156, 61–71. doi:10.1016/j.gexplo.2015.05.004
- Langman, J.B., Blowes, D.W., Veeramani, H., Wilson, D., Smith, L., Segó, D.C., Paktunc, D., 2015b. The mineral and aqueous phase evolution of sulfur and nickel with weathering of pyrrhotite in a low sulfide, granitic waste rock. *Chem. Geol.* 401, 169–179. doi:10.1016/j.chemgeo.2015.02.024
- Li, Y., Li, H., Yu, Y., Zhao, J., Wang, Y., Hu, C., Li, H., Wang, G., Li, Y., Gao, Y., 2018. Thiosulfate amendment reduces mercury accumulation in rice (*Oryza Sativa* L.). *Plant. Soil.* 430 (1-2), 413-422. doi: **10.1007/s11104-018-3726-2**
- Light, T.S., 1972. Standard solution for redox potential measurements. *Anal. Chem.* 44, 1038–1039. doi:10.1021/ac60314a021
- Liu, P., Ptacek, C.J., Blowes, D.W., Berti, W.R., Landis, R.C., 2015. Aqueous leaching of organic acids and dissolved organic carbon from various biochars prepared at different temperatures. *J. Environ. Qual.* 44, 684–695. doi:10.2134/jeq2014.08.0341
- Liu, P., Ptacek, C.J., Blowes, D.W., Landis, R.C., 2016. Mechanisms of mercury removal by biochars produced from different feedstocks determined using X-ray absorption spectroscopy. *J. Hazard. Mater.* 308, 233–242. doi:10.1016/j.jhazmat.2016.01.007
- Liu, P., Ptacek, C.J., Blowes, D.W., Gould, W.D. 2018. Control of mercury and methylmercury in contaminated sediments using biochar: A long-term microcosm study. *Appl. Geochem.* 92, 30-44. doi: 10.1016/j.apgeochem.2018.02.004
- Liu, P., Ptacek, C.J., Blowes, D.W., Finckh, Y.Z., Gordon, R.A., 2017. Stabilization of mercury in sediment by using biochars under reducing conditions. *J. Hazard. Mater.* 325, 120–128. doi:10.1016/j.jhazmat.2016.11.033
- Lowry, G. V., Shaw, S., Kim, C.S., Rytuba, J.J., Brown, G.E., 2004. Macroscopic and microscopic observations of particle-facilitated mercury transport from New Idria and Sulphur Bank mercury mine tailings. *Environ. Sci. Technol.* 38, 5101–5111. doi:10.1021/es034636c
- Maest, A., Nordstrom, D.K., 2017. A geochemical examination of humidity cell tests. *Appl. Geochem.* 81, 109-131. doi: .1016/j.apgeochem.2017.03.016
- Manceau, A., Marcus, M.A., Grangeon, S., 2012. Determination of Mn valence states in mixed-valent manganates by XANES spectroscopy. *Am. Mineral.* 97, 816–827. doi:10.2138/am.2012.3903
- Manceau, A., Nagy, K.L., 2012. Quantitative analysis of sulfur functional groups in natural organic matter by XANES spectroscopy. *Geochim. Cosmochim. Acta* 99, 206–223. doi:10.1016/j.gca.2012.09.033

- Manceau, A., Lemouchi, C., Enescu, M., Gaillot, A., Lanson, M., Magin, V., Glatzel, P., Poulin, B.A., Ryan, J.N., Aiken, G.R., Gautier-Luneau, I., Nagy, K., 2015. Formation of mercury sulfide from Hg(II)-thiolate complex in natural organic matter. *Environ. Sci. Technol.* 49 (16), 9787-9796. doi: 10.1021/acs.est.5b02522
- Montgomery, D.C., 2012. Simple comparative experiments, in: *Design and Analysis of Experiments*. John Wiley & Sons, Inc., Hoboken, NJ, pp. 25–59.
- Mosher, J.J., Vishnivetskaya, T.A., Elias, D.A., Podar, M., Brooks, S.C., Brown, S.D., Brandt, C.C., Palumbo, A. V., 2012. Characterization of the Deltaproteobacteria in contaminated and uncontaminated stream sediments and identification of potential mercury methylators. *Aquat. Microb. Ecol.* 66, 271–282. doi:10.3354/ame01563
- Morway, E.D., Thodal, C.E., Marvin-Dipasquale, M., 2017. Long-term trends of surface-water mercury and methylmercury concentrations downstream of historic mining within the Carson River watershed. *Eviron. Pollut.* 229, 1006-1018. doi:10.1016/j.envpol.2017.07.090
- Mucci, A., Bernier, G., Guignard, C., 2015. Mercury remobilization in Saguenay Fjord (Quebec, Canada) sediments: Insights following a mass-flow event and its capping efficiency. *Appl. Geochem.* 54, 13–26. doi:10.1016/j.apgeochem.2014.12.008
- Nordstrom, D.K., 1977. Thermochemical redox equilibria of ZoBell's solution. *Geochim. Cosmochim. Acta* 41, 1835–1841. doi:10.1016/0016-7037(77)90215-0
- Paulson, K.M.A., 2014. Methylmercury production in riverbank sediments of the South River, Virginia (USA) and assessment of biochar as a mercury treatment option. MSc Thesis, Earth Sciences, University of Waterloo, Waterloo, ON, Canada.
- Paulson, K.M.A., Ptacek, C.J., Blowes, D.W., Gould, W.D., Ma, J., Landis, R.C., Dyer, J.A., 2016. Role of organic carbon sources and sulfate in controlling net methylmercury production in riverbank sediments of the South River, VA (USA). *Geomicrobiology J.* 0, 1–14. doi:10.1080/01490451.2016.1247483
- Persson, I., Eriksson, L., Lindqvist-Reis, P., Persson, P., Sandstrom, M., 2008. An EXAFS spectroscopic, large-angle X-ray scattering, and crystallographic study of hexahydrated, dimethyl sulfoxide and pyridine 1-oxide hexasolvated mercury(II) ions. *Chem. Eur. J.* 14, 6687–6696. doi:10.1002/chem.200800225
- Pizzuto, J., 2012. Predicting the accumulation of mercury-contaminated sediment on riverbanks-An analytical approach. *Water Resour. Res.* 48, 1–13. doi:10.1029/2012WR011906
- Poulin, B.A., Aiken, G.R., Nagy, K.L., Manceau, A., Krabbenhoft, D.P., Ryan, J.N., 2016. Mercury transformation and release differs with depth and time in a contaminated riparian soil during simulated flooding. *Geochim. Cosmochim. Acta* 176, 118–138. doi:10.1016/j.gca.2015.12.024
- Prietzl, J., Thieme, J., Neuhäusler, U., Susini, J., Kögel-Knabner, I., 2003. Speciation of sulphur in soils and soil particles by X-ray spectromicroscopy. *Eur. J. Soil Sci.* 54, 423–433. doi:10.1046/j.1365-2389.2003.00543.x
- Ravel, B., Newville, M., 2005. ATHENA, ARTEMIS, HEPHAESTUS: Data analysis for X-ray absorption spectroscopy using IFEFFIT. *J. Synchrotron Radiat.* 12, 537–541. doi:10.1107/S0909049505012719
- Reardon, J., Foreman, J.A., Searcy, R.L., 1966. New reactants for the colorimetric determination of ammonia. *Clin. Chim. Acta* 14, 403–405. doi: 10.1016/0009-8981(66)90120-3

- Rhoades, E.L., O'Neal, M. a., Pizzuto, J.E., 2009. Quantifying bank erosion on the South River from 1937 to 2005, and its importance in assessing Hg contamination. *Appl. Geogr.* 29, 125–134. doi:10.1016/j.apgeog.2008.08.005
- Rimondi, V., Bardelli, F., Benvenuti, M., Costagliola, P., Gray, J.E., Lattanzi, P., 2014. Mercury speciation in the Mt. Amiata mining district (Italy): Interplay between urban activities and mercury contamination. *Chem. Geol.* 380, 110–118. doi:10.1016/j.chemgeo.2014.04.023
- Santoro, A., Terzano, R., Blo, G., Fiore, S., Mangold, S., Ruggiero, P., 2010. Mercury speciation in the colloidal fraction of a soil polluted by a chlor-alkali plant: A case study in the South of Italy. *J. Synchrotron Radiat.* 17, 187–192. doi:10.1107/S0909049510002001
- Singer, M.B., Harrison, L.R., Donovan, P. M., Blue, J.D., Marvin-DiPasquale, M., 2016. Hydrologic indicators of hot spot and hot moments of mercury methylation potential along river corridors. *Sci. Total. Environ.* 568, 691-711. doi:10.1016/j.scitotenv.2016.03.005
- Soil Survey Division Staff., 1993. *Soil Survey Manual*. U.S. Govt. Printing Office. Retrieved 25 September 2018.
- Terzano, R., Santoro, A., Spagnuolo, M., Vekemans, B., Medici, L., Janssens, K., Göttlicher, J., Denecke, M.A., Mangold, S., 2010. Solving mercury (Hg) speciation in soil samples by synchrotron X-ray microspectroscopic techniques. *Environ. Pollut.* 158, 2702–2709. doi:10.1016/j.envpol.2010.04.016
- Uchimiya, M., Bannon, D.I., Wartelle, L.H., 2012. Retention of heavy metals by carboxyl functional groups of biochars in small arms range soil. *J. Agric. Food Chem.* 60, 1798–1809. doi: 10.1021/jf2047898
- US EPA, 2009. Method 415.3, Revision 1.2: Determination of total organic carbon and specific UV absorbance at 254 nm in source water and drinking water. EPA/600/R-09/122.
- US EPA, 2002. Method 1631, Revision E: Mercury in water by oxidation, purge and trap, and cold vapor atomic fluorescence spectrometry. EPA-821-R-02-019 38.
- US EPA, 2001. Method 1630: Methyl mercury in water by distillation, aqueous ethylation, purge and trap, and CVAFS. EPA-821-R-01-020.
- Waldo, G.S., Carlson, R.M.K., Moldowan, J.M., Peters, K.E., Penner-hahn, J.E., 1991. Sulfur speciation in heavy petroleums: Information from X-ray absorption near-edge structure. *Geochim. Cosmochim. Acta* 55, 801–814. doi:10.1016/0016-7037(91)90343-4.
- Wang, J., Xing, Y., Xie, Y., Meng, Y., Xia, J., Feng, X., 2019. The use of calcium carbonate-enriched clay minerals and diammonium phosphate as novel immobilization agents for mercury remediation: Spectral investigations and field applications. *Sci. Total. Environ.* 646, 1615-1623. doi: 10.1016/j.scitotenv.2018.07.225
- Wilson, D., Amos, R.T., Blowes, D.W., Langman, J.B., Smith, L., Sego, D.C., 2018. Diavik waste rock project: Scale-up of a reactive transport model for temperature and sulfide-content dependent geochemical evolution of waste rock. *Appl. Geochem.* 96, 177-190
- Yu, R.-Q., Flanders, J.R., Mack, E.E., Turner, R., Mirza, M.B., Barkay, T., 2012. Contribution of coexisting sulfate and iron reducing bacteria to methylmercury

production in freshwater river sediments. *Environ. Sci. Technol.* 46, 2684–2691. doi: 10.1021/es2033718

Zhang, Y., Liu, Y., Lei, P., Wang, Y., Zhong, H., 2018. Biochar and nitrate reduce risk of methylmercury in soils under straw amendment. *Sci. Total. Environ.* 619-620, 384-390. doi: 10.1016/j.scitotenv.2017.11.106

ACCEPTED MANUSCRIPT

Figure 1 Schematic diagram of experimental design.

Figure 2 Concentrations of unfiltered Hg (orange diamonds) and 0.45- $\mu\text{m}$  filtered Hg (blue circles) in the effluent of treatment humidity columns (THC-HMT and THC-H6S) containing biochar. Dashed lines represent the concentration of Hg in the input solutions for the treatment columns. The input solutions were obtained by leaching floodplain soil MOTO (HMT) and riverbank sediment SR6 (H6S).

Figure 3 Concentrations of methylmercury (MeHg) in 0.45- $\mu\text{m}$  filtered effluent samples for treatment columns THC-HMT (blue circles) and THC-H6S (crosshairs).

Figure 4 Mean Hg concentrations and percentages extracted from the five-step sequential extraction for biochar collected at different depths from the treatment columns at the termination of the experiments using input derived from source columns HMT and H6S.

Figure 5 Concentration of solid-phase MeHg in biochar samples versus depth after termination of humidity cell experiments using input derived from source columns HMT and H6S. Error bars show the results of the first standard deviation of duplicate extractions at each depth.

Figure 6 Transmitted light microscope image and normalized  $\mu\text{-XRF}$  maps for Si, S, Fe, Cu, and Hg (a) obtained from the hardwood biochar collected from 0-2 cm of treatment column THC-HMT, and the corresponding XRF spectra obtained from the location denoted by ( $\square$ ) for lighter elements (b) and heavier elements (c).

Figure 7 Hg LIII-edge  $\mu\text{-XANES}$  analyses for biochar collected at depths 0-2 cm in THC-HMT. a.  $\mu\text{-XRF}$  map for Hg showing selected area for collecting  $\mu\text{-XANES}$ . b. Normalized Hg LIII-edge  $\mu\text{-XANES}$  (black solid line) and reference compounds (blue dash-dot line). c. best-fit (orange dashed line) (NSS = 0.02) in derivative using the three reference compounds.

Figure 8 Sulfur K-edge spectra (a) for the unused biochar and biochar after treatment at the different depths (in cm) from treatment columns THC-HMT and THC-H6S. Examples showing Gaussian peak fittings (orange dashed line) between 2,466 and 2,489 eV for fresh hardwood biochar (b, NSS =  $6.5 \times 10^{-3}$ ), and biochar collected from 0-2 cm in THC-HMT (c, NSS =  $3.9 \times 10^{-3}$ ) and THC-H6S (d, NSS =  $2.8 \times 10^{-3}$ ). Two optimized arctangent steps (black dash-dot line) were used to simulate reduced sulfur groups at 2,474 eV and oxidized sulfur groups at 2,482.5 eV. The grey solid lines

indicated white line positions for sulfide (2,470.4 eV, 2,472.3 eV), exocyclic sulfide (2,473.5 eV), heterocyclic S (2,474 eV), sulfoxide (2,476.1 eV), sulfone (2,480.2 eV), sulfonate (2,481.4 eV), and sulfate (2,482.7 eV).

Figure 9 Results of quantified S K-edge XANES using Gaussian peak fitting (a, c) and linear combination fitting (b, d) for the unused biochar and the biochar collected from treatment columns THC-HMT and THC-H6S.

ACCEPTED MANUSCRIPT

Table 1 Mean chemical compositions of effluents released from source columns (HMT and H6S) and treatment columns (THC-HMT, THC-H6S) over 100 weeks. Value represents mean +/- variance.

Parameter	HMT	THC-HMT	H6S	THC-H6S
pH	5.59 +/- 0.99	7.79 +/- 0.58	7.81 +/- 0.20	8.01 +/- 0.41
Eh, mV	539 +/- 87	470 +/- 78	427 +/- 42	424 +/- 74
Alkalinity, mg L <sup>-1</sup> (as CaCO <sub>3</sub> )	5 +/- 4	63 +/- 45	89.83 +/- 43.19	116 +/- 38
Dissolved organic carbon, mg L <sup>-1</sup>	5.31 +/- 1.47	2.89 +/- 0.66	2.912 +/- 0.468	3.99 +/- 2.09
Lactate, mg L <sup>-1</sup>	< 0.06	< 0.06	< 0.03	< 0.06
Acetate, mg L <sup>-1</sup>	< 0.6	< 0.2	< 0.08	< 0.3
Propionate, mg L <sup>-1</sup>	< 0.07	< 0.07	< 0.07	< 0.07
Formate, mg L <sup>-1</sup>	< 0.06	< 0.06	< 0.03	< 0.06
0.45- $\mu$ m filtered THg, ng L <sup>-1</sup>	3,180 +/- 1,510	541 +/- 227	472 +/- 79.1	151 +/- 75
unfiltered THg, ng L <sup>-1</sup>	27,000 +/- 11,400	7,700 +/- 861	11,200 +/- 11,400	538 +/- 241
F <sup>-</sup> , mg L <sup>-1</sup>	0.02 +/- 0.01	0.05 +/- 0.11	0.08 +/- 0.01	0.10 +/- 0.01
Cl <sup>-</sup> , mg L <sup>-1</sup>	0.26 +/- 0.26	1.25 +/- 1.36	5.70 +/- 0.68	6.70 +/- 1.0
NO <sub>2</sub> <sup>-</sup> , mg L <sup>-1</sup>	< 0.09	0.70 +/- 1.34	< 0.09	< 2
Br <sup>-</sup> , mg L <sup>-1</sup>	< 0.4	1.02 +/- 1.42	< 0.4	< 0.4
NO <sub>3</sub> <sup>-</sup> , mg L <sup>-1</sup>	4.83 +/- 3.11	4.83 +/- 2.65	4.01 +/- 2.23	1.40 +/- 0.60
SO <sub>4</sub> <sup>2-</sup> , mg L <sup>-1</sup>	2.48 +/- 0.35	5.54 +/- 1.62	7.87 +/- 1.54	10.3 +/- 2.40
Na, mg L <sup>-1</sup>	2.93 +/- 1.76	0.19 +/- 0.19	4.20 +/- 0.51	3.52 +/- 1.09
Mg, mg L <sup>-1</sup>	1.25 +/- 0.38	1.75 +/- 0.89	4.66 +/- 0.86	7.40 +/- 0.75
Al, $\mu$ g L <sup>-1</sup>	44.3 +/- 20.0	18.3 +/- 25.3	2.75 +/- 0.59	13.8 +/- 11.6
Si, mg L <sup>-1</sup>	3.20 +/- 0.81	2.82 +/- 0.59	9.66 +/- 0.55	6.63 +/- 1.08
Ca, mg L <sup>-1</sup>	9.63 +/- 2.64	5.42 +/- 12.6	58.0 +/- 1.61	37.5 +/- 5.4
K, mg L <sup>-1</sup>	1.68 +/- 0.98	14.8 +/- 30.2	1.95 +/- 0.46	20.8 +/- 34.1
MeHg, ng L <sup>-1</sup>	1.62 +/- 1.76	0.38 +/- 0.23	0.28 +/- 0.16	0.11 +/- 0.02

Table 2 Mean total Hg retained on biochar obtained from the differences of unfiltered Hg in effluent from source and treatment columns and normalized to mass of biochar in treatment columns.

Reactive Material in Humidity Cells	THC-HMT	THC-H6S
Hg loaded on biochar ( $\mu\text{g g}^{-1}$ )	7.96	2.38
Cumulative Hg eluted ( $\mu\text{g g}^{-1}$ )	1.52	0.09
Hg retained on biochar ( $\mu\text{g g}^{-1}$ )	6.44	2.29
Percent Hg retained on biochar	81.3%	96.2%

## Highlights

- Biochar stabilized particulate and dissolved Hg derived from riverine sediments
- >80% Hg stabilized on the biochar without promoting methylation reactions
- Both physical and chemical processes control Hg removal

ACCEPTED MANUSCRIPT

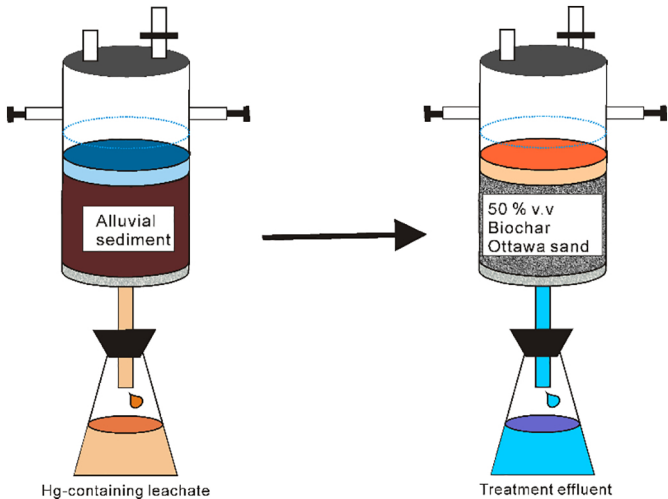


Figure 1

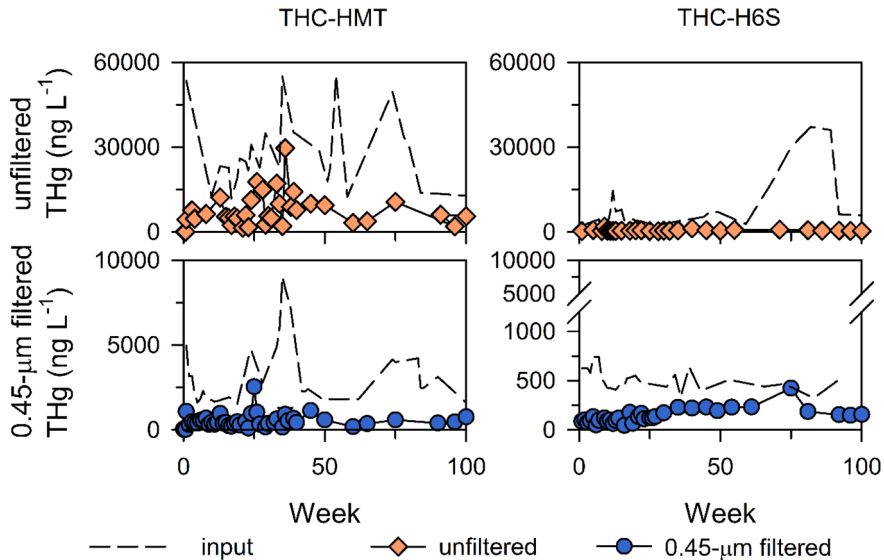


Figure 2

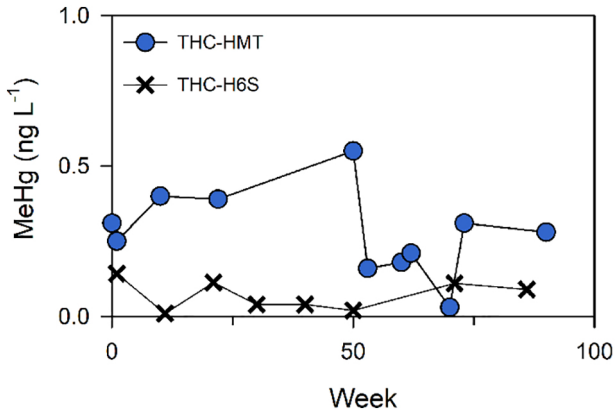


Figure 3

THC-HMT

THC-H6S

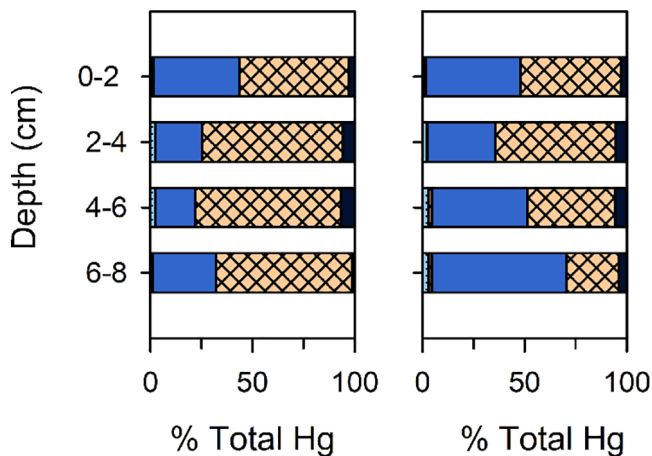
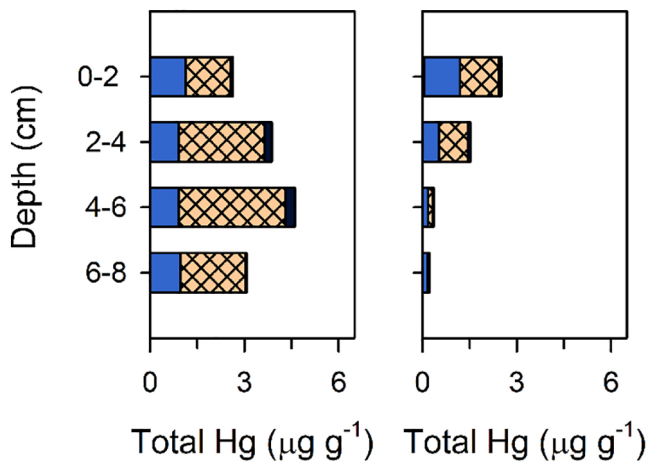


Figure 4

Depth (cm)

THC-HMT

THC-H6S

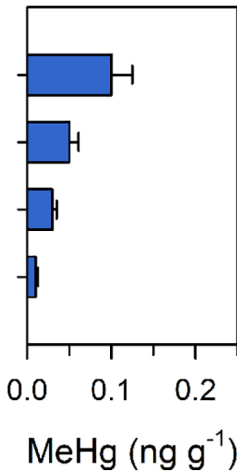
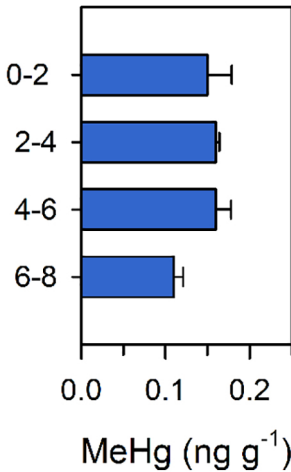


Figure 5

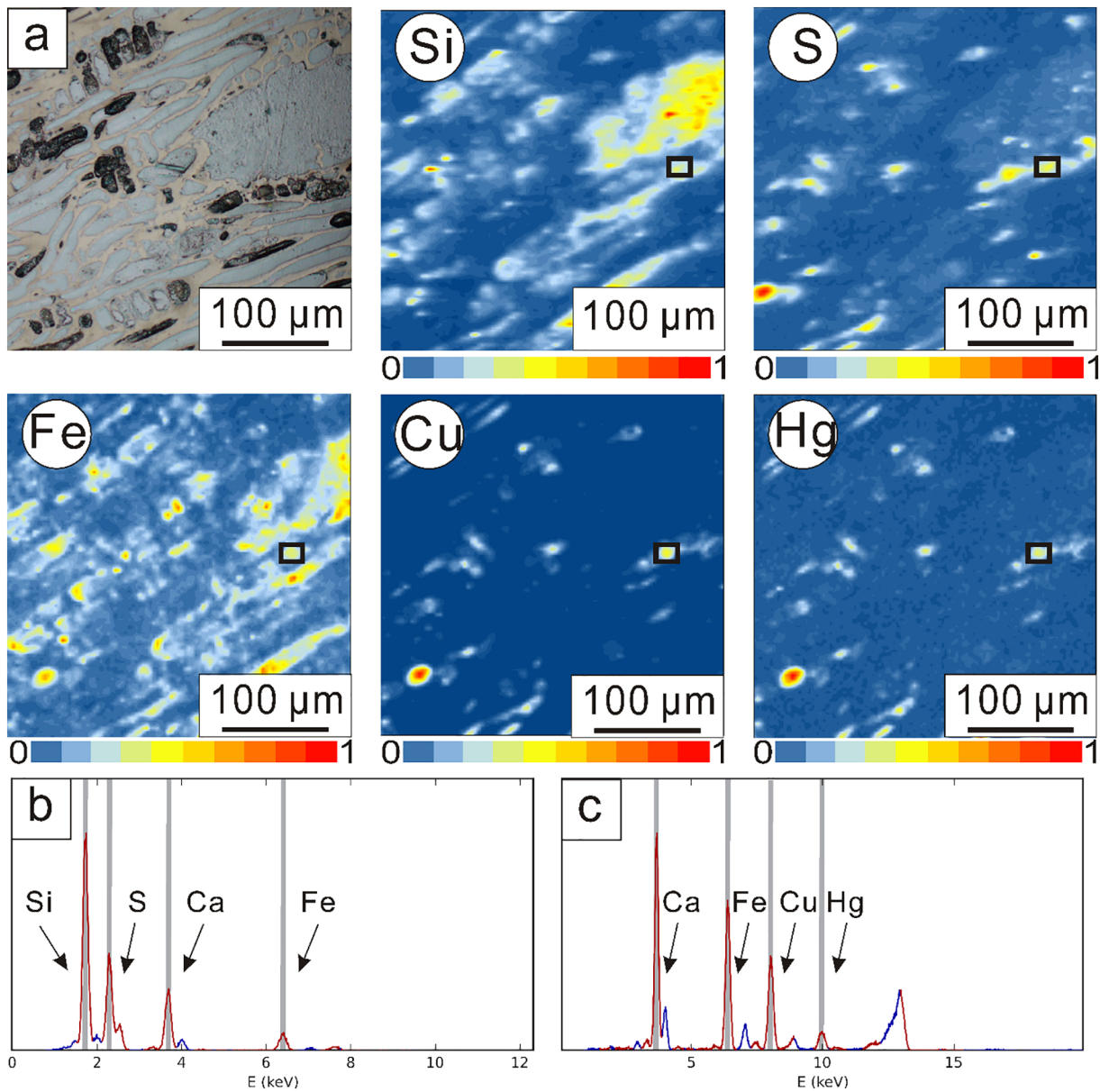


Figure 6

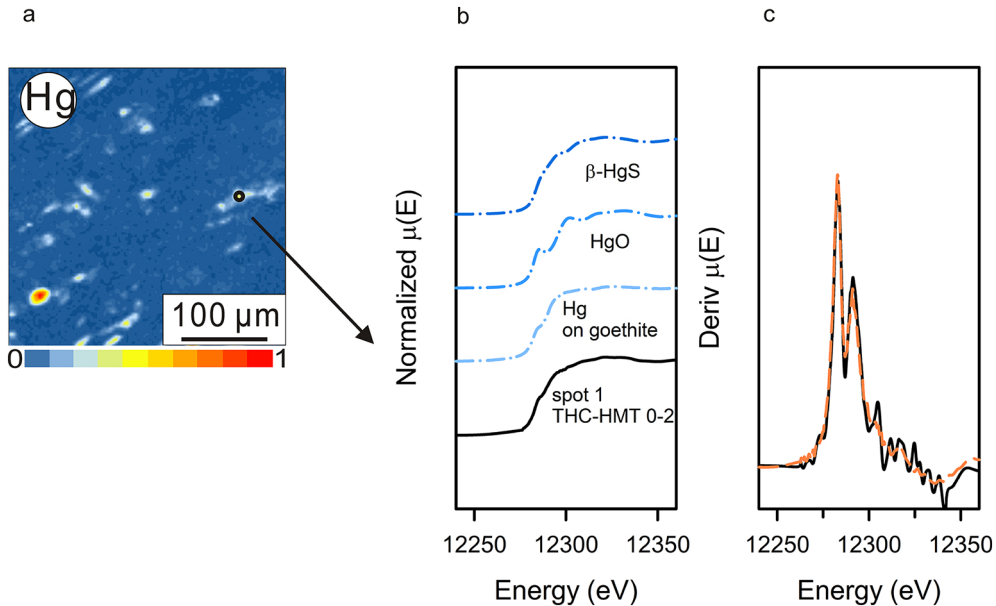


Figure 7

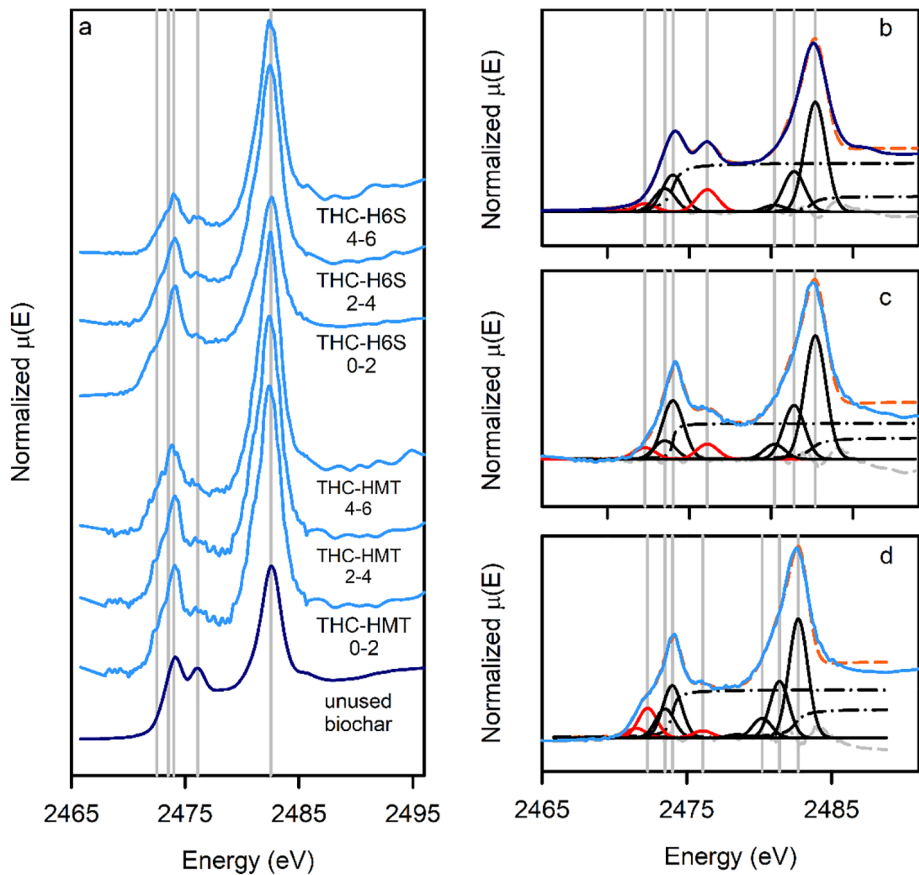


Figure 8

## THC-HMT

## THC-H6S

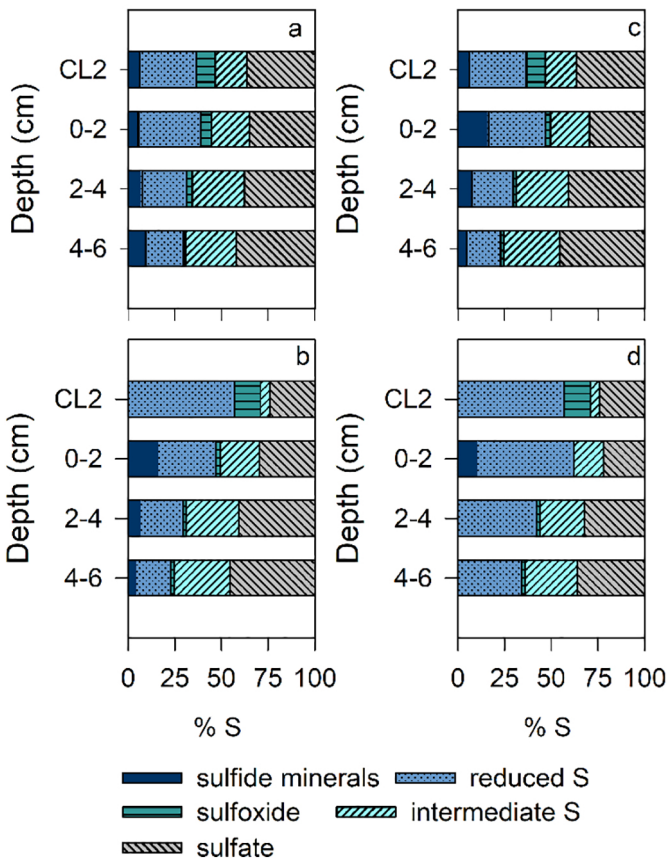


Figure 9